The Computer Journal Advance Access published December 10, 2007

doi:10.1093/comjnl/bxm098

Super-Resolution and Blind Deconvolution For Rational Factors With an Application to Color Images

FILIP ŠROUBEK[1,*], JAN FLUSSER[1] AND GABRIEL CRISTÓBAL[2]

[1]*Institute of Information Theory and Automation, AS CR, Pod vodárenskou věží 4, 182 08, Prague 8, Czech Republic*
[2]*Instituto de Óptica, CSIC, Serrano 121, 28006 Madrid, Spain*
**Corresponding author: sroubekf@utia.cas.cz*

In many real applications, traditional super-resolution (SR) methods fail to provide high-resolution images due to objectionable blur and inaccurate registration of input low-resolution images. Only integer resolution enhancement factors, such as 2 or 3, are often considered, but non-integer factors between 1 and 2 are also important in real cases. We introduce a method to SR and deconvolution, which assumes no prior information about the shape of degradation blurs, incorporates registration parameters, and is properly defined for any rational (fractional) resolution factor. The method minimizes a regularized energy function with respect to the high-resolution image and blurs, where regularization is carried out in both the image and blur domains. The blur regularization is based on a generalized multi-channel blind deconvolution constraint derived in the paper. An extension to color images is briefly discussed. Experiments on real data illustrate robustness to noise and other advantages of the method.

Keywords: super-resolution; blind deconvolution; alternating minimization; polyphase components

Received 19 December 2006; revised 24 October 2007

1. INTRODUCTION

Imaging devices have limited achievable resolution due to many theoretical and practical restrictions. An original scene with a continuous intensity function $o(x, y)$ warps at the camera lens because of the scene motion and/or the change of the camera position. In addition, several external effects blur images: atmospheric turbulence, camera lens, relative camera-scene motion, etc. We will call these effects *volatile blurs* to emphasize their unpredictable and transitory behavior, yet we will assume that we can model them as convolution with an unknown point spread function (PSF) $v(x, y)$. This is a reasonable assumption if the original scene is flat and perpendicular to the optical axis. Finally, charge-coupled devices (CCDs) discretize the image and produces digitized noisy image $g(i, j)$, which we refer to as a *low-resolution* (LR) *image*, since the spatial resolution is too low to capture all the details of the original scene. For one single observation $g(i, j)$, the problem is heavily underdetermined and lacks stable solution. To partially overcome the equivocation of the problem, we can take K ($K > 1$) images of the original scene and face the so-called multi-channel (multi-frame) problem. The acquisition model then becomes

$$g_k(i, j) = D([v_k * W_k(o)](x, y)) + n_k(i, j) \tag{1}$$

where $k = 1, \ldots, K$ is the acquisition index, $n_k(i, j)$ the additive noise and W_k the geometric deformation (warping), in general different for each acquisition. $D(\cdot)$ is the *decimation operator* that models the function of CCD sensors. It consists of convolution with a *sensor PSF* followed by a *sampling operator*, which we define as multiplication by a sum of delta functions placed on a grid. The above model is the state of the art as it takes all possible degradations into account.

Super-resolution (SR) is the process of combining a sequence of LR images in order to produce an image or sequence of higher resolution. It is unrealistic to assume that the super-resolved image can recover the original scene $o(x, y)$ exactly. A reasonable goal of SR is a discrete version of $o(x, y)$, which has higher spatial resolution than the resolution of the LR images and which is free of the volatile blurs (deconvolved). In the paper, we will refer to this super-resolved image as a *high-resolution* (HR) *image* $f(i, j)$ and the ratio between the

size of the sought HR image and input LR image will be called an *SR factor* and denoted by ε. The standard SR approach consists of subpixel registration, overlaying the LR images on an HR grid, and interpolating the missing values. The subpixel shift between images thus constitutes an essential feature. We will demonstrate that considering volatile blurs in the model explicitly brings about a more general and robust technique, with the subpixel shift being a special case thereof.

The acquisition model in equation (1) embraces three distinct cases frequently encountered in the literature. First, removal of the geometric degradation W_k is a registration problem. Second, if the decimation operator D and the geometric transform W_k are not considered, then we face a *multi-channel* (or multi-frame) *blind deconvolution* (MBD) problem. Third, if the volatile blur v_k is not considered or assumed known, and W_k is suppressed except to subpixel translations, we obtain a classical SR formulation. In practice, it is crucial to consider all three cases at once. We are then confronted with a problem of *blind SR* (BSR), the topic of this paper.

Proper registration techniques can suppress large and complex geometric distortions but usually a small between-image shift is still observable. There have been hundreds of methods proposed; see e.g. [1] for a survey. Here, we will assume that registration parameters can be calculated by one of the methods, and if applied, the LR images are registered except to small translations.

Research on intrinsically MBD methods has begun fairly recently; refer to [2–6] for a survey and other references. The MBD methods can directly recover the blurring functions from the degraded images alone. We further developed the MBD theory in [7] by proposing a blind deconvolution method for images, which might be mutually shifted by unknown vectors. To make this brief survey complete, we should not forget to mention a very challenging problem of shift-variant blind deconvolution, that was considered in [8, 9].

A countless number of papers address the standard SR problem. A good survey can be found in [10, 11]. Maximum likelihood, maximum *a posteriori* (MAP), the set theoretic approach using projection on convex sets and fast Fourier techniques can all provide a solution to the SR problem. Earlier approaches assumed that subpixel shifts are estimated by other means. More advanced techniques, such as in [12–14], include the shift estimation in the SR process. Other approaches focus on fast implementation [15], space–time SR [16], SR with complex image priors for joint image and segmentation estimation [17] or SR of compressed video [13]. Most of the SR techniques assume *a priori* known blurs. However, in many cases, such as camera motion, blurs can have wild shapes that are difficult to predict; see examples of real motion blurs in [18]. Nguyen *et al.* [19], Woods *et al.* [20] and Rajan and Chaudhuri [21] proposed BSR that can handle parametric PSFs, i.e. PSFs modeled with one parameter. This restriction is unfortunately very limiting for most real applications. In [22], we extended our MBD method to BSR in an intuitive way but one can prove that this approach does not estimate PSFs accurately. The same intuitive approach was also proposed in [23]. To our knowledge, first attempts for theoretically correct BSR with an arbitrary PSF appeared in [24,25]. The interesting idea proposed therein is to use the so-called polyphase components. We will adopt the same idea here as well. Other preliminary results of the BSR problem with focus on fast calculation are given in [26], where the authors propose a modification of the Richardson–Lucy algorithm.

Current MBD techniques require no or very little prior information about the blurs, they are sufficiently robust to noise and provide satisfying results in most real applications. However, they can hardly cope with the decimation operator, which violates the standard convolution model. On the contrary, state-of-the-art SR techniques achieve remarkable results of resolution enhancement in the case of no blur. They accurately estimate the subpixel shift between images but lack any apparatus to calculate the blurs.

Recently, in [27], we proposed a unifying method that simultaneously estimates the volatile blurs and HR image. The only prior knowledge required are estimates of the blur size and the level of noise in the LR images, which renders it a truly BSR method. The key idea was to determine subpixel shifts by calculating volatile blurs. As the volatile blurs are estimated in the HR scale, positions of their centroids correspond to sub pixel shifts. Therefore, by estimating blurs, we automatically estimate shifts with subpixel accuracy, which is essential for good performance of SR. This complex SR problem was solved by minimizing a regularized energy function, where the regularization was carried out in both the image and blur domains. The image regularization is based on variational integrals, and a consequent anisotropic diffusion with good edge-preserving capabilities. The blur regularization term is based on our generalized result of blur estimation in the SR case. To tackle the minimization task, we used an alternating minimization (AM) approach consisting of two simple linear equations.

In this work, we extend the BSR method by incorporating registration parameters and color images. To address correctly the correlation of color channels, we apply the regularizations proposed in [28]. Further, we show that by using the polyphase decomposition, we can formulate the SR problem not only for integer factors but also for any rational (fractional) factor, which is important in real applications where often only an SR factor between 1 and 2 is possible. If the noise removal and registration steps are not sufficiently reliable, a factor of 1.6 is the practical limit of SR [29]. The need for rational factors in SR was also reported in [30] with a focus on fast calculation using preconditioners.

Section 2 outlines the degradation model in the discrete domain for integer and non-integer SR factors. In Section 3, we present the regularized energy functional, derive the regularization terms and sketch an extension to color images.

The AM scheme and parameter estimation is given in Section 4. Finally, Section 5 illustrates the applicability of the proposed method to real situations.

2. DISCRETE MODEL

To simplify the notation, we will assume only images and PSFs with square supports. An extension to rectangular images is straightforward. Let $f(i, j)$ be an arbitrary discrete image of size $F \times F$ then $\mathbf{f}$ denotes an image column vector of size $F^2 \times 1$ and $\mathbf{C}_A\{f\}$ denotes a matrix that performs convolution of f with an image of size $A \times A$. The convolution matrix can have a different output size. Adopting the Matlab naming convention, we distinguish two cases: 'full' convolution $\mathbf{C}_A\{f\}$ of size $(F + A - 1)^2 \times A^2$ and 'valid' convolution $\mathbf{C}_A^v\{f\}$ of size $(F - A + 1)^2 \times A^2$. In both cases, the convolution matrix is of the Toeplitz-block-Toeplitz form. In the paper, we will not specify dimensions of convolution matrices if it is obvious from the size of the right argument.

Before we proceed, it is necessary to define precisely the *sampling matrix* $\mathbf{S}$. Let $\mathbf{S}^\varepsilon$ denote an 1-D sampling matrix, where ε is the integer subsampling factor and $i = 1,\ldots,\varepsilon$. Each row of the sampling matrix is a unit vector whose non-zero element is at such position that, if the matrix multiplies an arbitrary vector b, the result of the product is every εth element of b starting from b_i. If the vector length is M then the size of the sampling matrix is $\lceil (M - i + 1)/\varepsilon \rceil \times M$, where $\lceil \cdot \rceil$ rounds up to the closest integer. A 2-D sampling matrix is defined by

$$\mathbf{S}_{i,j}^\varepsilon := \mathbf{S}_i^\varepsilon \otimes \mathbf{S}_j^\varepsilon, \tag{2}$$

where $\otimes$ denotes the matrix direct product (Kronecker product operator). If the starting index (i, j) will be (1, 1) then we will omit the subscript and simply write $\mathbf{S}^\varepsilon$. Note that the transposed matrix $(\mathbf{S}^\varepsilon)^{\mathrm{T}}$ behaves as an upsampling operator that interlaces the original samples with $(\varepsilon - 1)$ zeros.

Polyphase components of an image $f(x, y)$ are

$$\mathbf{f}^{ij} := \mathbf{S}_{i,j}^\varepsilon \mathbf{f} \tag{3}$$

which is equivalent to

$$\mathbf{f}^{ij} := [f[i, j], f[i + \varepsilon, j], f[i + 2\varepsilon, j], \ldots, f[i, j + \varepsilon], f[i + \varepsilon, j + \varepsilon], \ldots]^{\mathrm{T}}.$$

Therefore, each image breaks into ε^2 distinct polyphase components (downsampled versions of the image) (see Fig. 1).

Let us now define a discrete version of the acquisition model in equation (1). Assume that we have K different LR frames $\{g_k\}$ (each of size $G \times G$) that represent degraded (blurred and noisy) versions of the original scene. Our goal is to estimate the HR representation of the original scene, which we denoted as the HR image f of size $F \times F$. The LR frames are linked with the HR image through a series of degradations similar to those between $o(x, y)$ and g_k in equation (1). First f is geometrically warped ($\mathbf{W}_k$), then it is convolved with a volatile PSF ($\mathbf{V}_k$) and finally it is decimated ($\mathbf{D}$). The decimation operator $\mathbf{D}$ depends only on sensor characteristics and since we assume the same sensor in all acquisitions it appears without the index k. The formation of the LR images in vector–matrix notation is then described as

$$\mathbf{g}_k = \mathbf{D}\mathbf{V}_k\mathbf{W}_k\mathbf{f} + \mathbf{n}_k, \tag{4}$$

where $\mathbf{n}_k$ is additive noise present in every channel. In principle, $\mathbf{W}_k$ can be a very complex geometric transform that must be estimated by image registration or motion detection techniques. We have to keep in mind that the subpixel accuracy in $\mathbf{g}_k$'s is essential for SR to work properly. Standard image registration techniques can hardly achieve this and they leave a small misalignment behind. Then the warping operator splits into $\mathbf{W}_k = \mathbf{T}_k\mathbf{W}_k'$, where $\mathbf{W}_k'$ is estimated by some registration methods and $\mathbf{T}_k$ is the unknown translation. In order to change the order of geometrical warping and convolution, we consider only linear transformations. Unknown translation $\mathbf{T}_k$ combined with volatile PSF $\mathbf{V}_k$ gives us $\mathbf{V}_k\mathbf{T}_k = \mathbf{H}_k$, where $\mathbf{H}_k$ performs convolution with the shifted version of the volatile PSF v_k. The decimation matrix $\mathbf{D} = \mathbf{S}^\varepsilon\mathbf{U}$ simulates the behavior of digital sensors by first performing convolution with the $U \times U$ sensor PSF ($\mathbf{U}$) and then downsampling ($\mathbf{S}^\varepsilon$) by factor ε. Assuming linear transformations, $\mathbf{W}_k'$ may be grouped with the decimation operator resulting in $\mathbf{D}_k = \mathbf{S}^\varepsilon\,\mathbf{U}\mathbf{W}_k'$. From the numerical point of view, it is preferable to construct directly the whole $\mathbf{D}_k$ than the individual matrices $\mathbf{S}^\varepsilon$, $\mathbf{U}$ and $\mathbf{W}_k'$. Finally, the acquisition model reads

$$\mathbf{g}_k = \mathbf{D}_k\mathbf{H}_k\mathbf{f} + \mathbf{n}_k = \mathbf{S}^\varepsilon\mathbf{U}\mathbf{W}_k'\mathbf{H}_k\mathbf{f} + \mathbf{n}_k. \tag{5}$$

The BSR problem we are solving is the following: we know the LR images $\{g_k\}$ and $\mathbf{D}_k$'s, and we want to estimate the HR

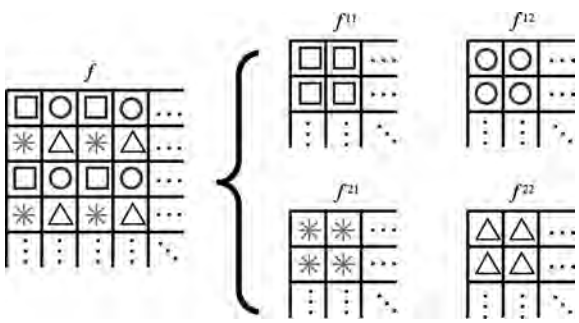

FIGURE 1. Polyphase decomposition for $\varepsilon = 2$: original image f decomposes into four downsampled images.

image f. In addition, the rough estimates of the size of volatile blur h_k and of the noise variance σ_n is necessary. PSFs h_k can be of different size. However, we postulate that they all fit into an $H \times H$ support. To avoid boundary effects, we assume that each observation g_k captures only a part of f. Hence, $\mathbf{H}_k$ and $\mathbf{U}$ are 'valid' convolution matrices $\mathbf{C}^v_F\{h_k\}$ and $\mathbf{C}^v_{F-H+1}\{u\}$, respectively.

To be able to deal correctly with non-integer SR factors, we need to express the above model using a sampling operator with integer ε. This will be necessary in the derivation of blur regularization in the next section. It can be done for factors expressed as a fraction p/q, where p and q are positive integers and $p > q$ (p and q are reduced so that they do not have any common factor).

Let $\varepsilon = p/q$ and the sampling frequency of the LR images g_k be q, then the sampling frequency (number of pixels per unit distance) of the HR image f is p. From each LR image g_k, we generate q^2 polyphase components. We consider these polyphase components as new input (downsampled-LR) images with the sampling frequency 1. Now, to obtain the HR image from the downsampled-LR images, we must solve an SR problem with the integer factor $\varepsilon = p$ and not with the rational one as before. In other words, in order to obtained an integer SR factor we downsample the LR images and thus artificially increase the number of channels. However, the number of unknown PSFs h_k remains the same. We still have K PSFs since every pack of q^2 downsampled-LR images contains the same blur.

An equivalent formulation of the model in equation (5) but for fractional SR factors p/q is

$$\begin{bmatrix} \mathbf{g}_k^{11} \\ \vdots \\ \mathbf{g}_k^{qq} \end{bmatrix} = \begin{bmatrix} \mathbf{S}^p\mathbf{U}_{1,1} \\ \vdots \\ \mathbf{S}^p\mathbf{U}_{q,q} \end{bmatrix} \mathbf{W}'_k\mathbf{H}_k\mathbf{f} + \mathbf{n}_k, \tag{6}$$

where each $\mathbf{U}_{i,j}$ performs convolution with one of the q^2 discretizations of the sensor PSF u and $\mathbf{g}_k^{ij} = \mathbf{S}^g_{i,j}\mathbf{g}_k$ are polyphase components of g_k for SR factor q. It is important to understand the discretization of the sensor PSF u in the case of fractional SR factors. Since p is not divisible by q, the product $\mathbf{S}^\varepsilon\mathbf{U}$ is shift-variant and it depends on a relative shift between the HR and LR pixels. One can readily see that the relative shift repeats every qth pixels (in both directions x and y) of the LR image and therefore we have q^2 distinct PSF discretizations. For further details see [31].

3. BLIND SUPERRESOLUTION

In order to solve the BSR problem, i.e. determine the HR image f and volatile PSFs h_k, we adopt an approach of minimizing a regularized energy function. This way the method will be less vulnerable to noise and better posed. The energy consists of three terms and takes the form

$$E(\mathbf{f}, \mathbf{h}) = \sum_{k=1}^{K} \|\mathbf{D}_k\mathbf{H}_k\mathbf{f} - \mathbf{g}_k\|^2 + Q(\mathbf{f}) + R(\mathbf{h}), \tag{7}$$

where $\mathbf{h} = [\mathbf{h}_1^{\mathrm{T}}, \ldots, \mathbf{h}_K^{\mathrm{T}}]^{\mathrm{T}}$. The first term measures the fidelity to the data and emanates from our acquisition model (5). The remaining two are regularization terms that attract the minimum of E to an admissible set of solutions. The form of E very much resembles the energy proposed in [7] for MBD. Indeed, this should not come as a surprise since MBD and SR are related problems in our formulation.

3.1. Image regularization

Regularization $Q(\mathbf{f})$ is a smoothing term of the form

$$Q(\mathbf{f}) = \alpha\mathbf{f}^{\mathrm{T}}\mathbf{L}\mathbf{f}, \tag{8}$$

where $\mathbf{L}$ is a high-pass filter and α is a positive regularization parameter. A common strategy is to use convolution with the Laplacian for $\mathbf{L}$, which in the continuous case, corresponds to $Q(f) = \int |\nabla f|^2$. Recently, variational integrals $Q(f) = \int \phi(|\nabla f|)$ were proposed, where ϕ is a strictly convex, non-decreasing function that grows at most linearly. Examples of $\phi(s)$ are s (total variation), $\sqrt{1 + s^2 - 1}$ (hypersurface minimal function), $\log(\cosh(s))$ or non-convex functions, such as $\log(1 + s^2)$, $s^2/(1 + s^2)$ and $\arctan(s^2)$ (Mumford–Shah functional). The advantage of the variational approach is that while in smooth areas it has the same isotropic behavior as the Laplacian, it also preserves edges in images. The disadvantage is that it is highly nonlinear and to overcome this difficulty, one must use, e.g. half-quadratic algorithm [32]. For the purpose of our discussion, it suffices to state that after discretization we arrive again at equation (8), where this time $\mathbf{L}$ is a positive semi-definite block tridiagonal matrix constructed of values depending on the gradient of f. The rationale behind the choice of $Q(f)$ is to constrain the local spatial behavior of images; it resembles a Markov Random Field. Some global constraints may be more desirable but are difficult (often impossible) to define, since we develop a general method that should work with any class of images.

3.2. PSF regularization

Our PSF regularization term $R(\mathbf{h})$ consists of two terms. The first one is the same smoothing term as for images but applied to blurs, which is a typical prior that penalizes jagged blurs that are rare in real situations. The second term is a consistency term that binds the different volatile PSFs to prevent them from moving freely and unlike the fidelity term [the first term in equation (7)] it is based solely on the observed LR images. It takes the form of $\|\mathcal{N}\mathbf{h}\|^2$, where the

matrix $\mathcal{N}$ will be derived later. The complete PSF regularization is then given by

$$R(\mathbf{h}) = \beta \mathbf{h}^{\mathrm{T}} \mathbf{L} \mathbf{h} + \gamma \|\mathcal{N}\mathbf{h}\|^2, \tag{9}$$

where β and γ are positive regularization parameters that give different weights to the terms.

Consider the discrete model in equation (6) but without noise $\mathbf{n}_k$ and warping $\mathbf{W}_k'$ (this can be removed by registering the LR images). Let E be a positive integer and $\mathcal{G} := [\mathbf{G}_1^{11}, \ldots, \mathbf{G}_1^{qq}, \mathbf{G}_2^{11}, \ldots, \ldots, \mathbf{G}_K^{qq}]$, where $\mathbf{G}_k^{ij} := \mathbf{C}_E^v\{g_k^{ij}\}$. There are q^2 distinct discretizations of the sensor PSF u that depend on the relative shift between the HR and LR pixels. Let $u_{i,j}$ $(i, j = 1,\ldots,q)$ denote such discretizations.

Matrix $\mathcal{G}$ expressed in terms of f, u and h_k takes the form

$$\mathcal{G} = \mathbf{S}^p \mathbf{F}[\mathbf{U}_{1,1}, \ldots, \mathbf{U}_{q,q}]\mathcal{H}, \tag{10}$$

where $\mathbf{U}_{i,j} = \mathbf{C}_{pE-p+H}\{u_{i,j}\}$, $\mathbf{F} = \mathbf{C}^v_{pE-p+H+U-1}\{f\}$ and

$$\mathcal{H} := [\mathbf{I}_{q^2} \otimes (\mathbf{C}_{pE-p+1}\{h_1\}(\mathbf{S}^p)^{\mathrm{T}}), \ldots, \mathbf{I}_{q^2} \otimes (\mathbf{C}_{pE-p+1}\{h_K\} \times (\mathbf{S}^p)^{\mathrm{T}})].$$

The size of the upsampling matrix $(\mathbf{S}^p)^{\mathrm{T}}$ inside $\mathcal{H}$ is $(pE - p + 1)^2 \times E^2$.

If $\mathbf{S}^p\mathbf{F}$ is of full column rank, which is almost certainly true for real and sufficiently large images (see [31] for more details), then $\mathrm{Null}(\mathcal{G}) \equiv \mathrm{Null}([\mathbf{U}_{1,1}, \ldots, \mathbf{U}_{q,q}]\mathcal{H})$. The difference between the number of columns and rows of $[\mathbf{U}_{1,1}, \ldots, \mathbf{U}_{q,q}]\mathcal{H}$ bounds from below the dimension of $\mathcal{G}$'s null space, i.e.

$$\mathrm{nullity}(\mathcal{G}) \geq N := K(qE)^2 - (pE - p + H + U - 1)^2. \tag{11}$$

Let $\mathbf{N}$ denote N null vectors of $\mathcal{G}$ stacked column-wise and η_{kn} are some $E \times E$ filters. We can visualize $\mathbf{N}$ as

$$\mathbf{N} = \begin{bmatrix} \boldsymbol{\eta}_{1,1} & \cdots & \boldsymbol{\eta}_{1,N} \\ \vdots & \ddots & \vdots \\ \boldsymbol{\eta}_{q^2,1} & \cdots & \boldsymbol{\eta}_{q^2,N} \\ \vdots & \ddots & \vdots \\ \boldsymbol{\eta}_{Kq^2,1} & \cdots & \boldsymbol{\eta}_{Kq^2,N} \end{bmatrix}, \tag{12}$$

where $\boldsymbol{\eta}_{kn}$ is the vector representation of η_{kn}. Let $\tilde{\eta}_{kn}$ denote upsampled η_{kn} by factor p. Then

$$\mathcal{N} := \begin{bmatrix} \mathbf{C}_{U+H-1}\{\tilde{\eta}_{1,1}\} & \cdots & \mathbf{C}_{U+H-1}\{\tilde{\eta}_{Kq^2,1}\} \\ \vdots & \ddots & \vdots \\ \mathbf{C}_{U+H-1}\{\tilde{\eta}_{1,N}\} & \cdots & \mathbf{C}_{U+H-1}\{\tilde{\eta}_{Kq^2,N}\} \end{bmatrix} \times \mathbf{I}_K \otimes \begin{bmatrix} \mathbf{C}_H\{u_{1,1}\} \\ \vdots \\ \mathbf{C}_H\{u_{q,q}\} \end{bmatrix} \tag{13}$$

and we conclude (without proofs for the sake if simplicity) that

$$\mathcal{N}\mathbf{h} = \mathbf{0}. \tag{14}$$

An interesting observation follows from the nullity condition in equation (11): $K > (pE - p + H + U - 1)^2/(qE)^2$ and if $E \gg (p + H + U - 1)$ then $K > (p/q)^2$. It implies that the minimum number of input channels necessary for blur reconstruction to work is $K > \varepsilon^2$. For example, for $\varepsilon = 3/2$, three LR images are sufficient; for $\varepsilon = 2$, we need at least five LR images to perform blur reconstruction. Note that for no SR ($\varepsilon = 1$), the minimum number of input channels is 2, which is of course in accordance with the MBD theory.

To better understand the above derivation, the following example illustrates all the steps for an 1-D case.

EXAMPLE Let the HR signal be an 1-D periodic pulse f with the period [1, 1, 1, 1,0,0,0]. Such signal satisfies the necessary condition that $\mathbf{S}^p\mathbf{F}$ is of full-column rank. The HR signal is blurred by $h_1 = [0,1]$ and $h_2 = [1, 0]$ $(H = 2)$ and downsampled by factor $\varepsilon = p/q = 3/2$. To simplify the derivation, the sensor PSF u will be a pulse of length 1.5 HR pixels and its two $(q = 2)$ distinct discretizations are $u_1 = [0.5, 0.5, 0]$ and $u_2 = [0, 0, 1]$ $(U = 3)$ as depicted below:

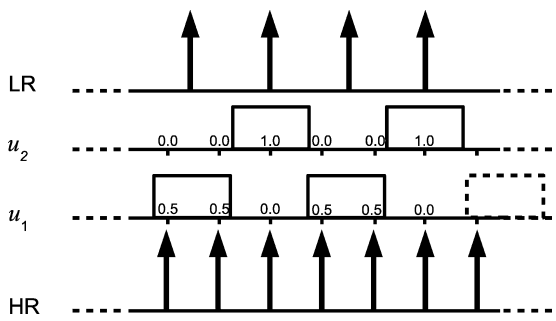

The two $(K = 2)$ measured LR signals are thus

$$g_1 = [1, 1, 0.5, 0, 0.5, 1, 1, 0, 0, 1, 1, 1, 0, 0, \ldots],$$
$$g_2 = [1, 1, 0, 0, 1, 1, 0.5, 0, 0.5, 1, 1, 0, 0, 1, \ldots]$$

and their two ($q = 2$) polyphase components are

$$\begin{array}{lllllllll} g_1^1 & = [1 & 0.5 & 0.5 & 1 & 0 & 1 & 0 & \ldots], \\ g_1^2 & = [1 & 0 & 1 & 0 & 1 & 1 & 0 & \ldots], \\ g_2^1 & = [1 & 0 & 1 & 0.5 & 0.5 & 1 & 0 & \ldots], \\ g_2^2 & = [1 & 0 & 1 & 0 & 1 & 0 & 1 & \ldots]. \end{array}$$

In the 1-D case, condition (11) reads nullity($\mathcal{G}$) $\geq N := K(qE) - (pE - p + H + U - 1)$. Therefore, for the minimum admissible nullity $N = 1$, the size of filters η must be $E = 2$. From the LR signals, we thus construct

$$\mathcal{G} = \begin{bmatrix} 0.5 & 1 & 0 & 1 & 0 & 1 & 0 & 1 \\ 0.5 & 0.5 & 1 & 0 & 1 & 0 & 1 & 0 \\ 1 & 0.5 & 0 & 1 & 0.5 & 1 & 0 & 1 \\ 0 & 1 & 1 & 0 & 0.5 & 0.5 & 1 & 0 \\ 1 & 0 & 1 & 1 & 1 & 0.5 & 0 & 1 \\ 0 & 1 & 0 & 1 & 0 & 1 & 1 & 0 \\ 1 & 0 & 1 & 0 & 1 & 0 & 1 & 1 \\ \vdots & \vdots & \vdots & \vdots & \vdots & \vdots & \vdots & \vdots \end{bmatrix}.$$

The null space of $\mathcal{G}$ is a single vector

$$\mathbf{N} = \begin{bmatrix} -0.6325 \\ 0 \\ -0.3162 \\ 0 \\ 0.6325 \\ 0 \\ 0 \\ 0.3162 \end{bmatrix}.$$

Extracting filters η's of length $E = 2$ from $\mathbf{N}$ and upsampling by $p = 3$, gives

$$\begin{array}{lllllll} \tilde{\eta}_{1,1} & = [& -0.6325 & 0 & 0 & 0 &], \\ \tilde{\eta}_{2,1} & = [& -0.3162 & 0 & 0 & 0 &], \\ \tilde{\eta}_{3,1} & = [& 0.6325 & 0 & 0 & 0 &], \\ \tilde{\eta}_{4,1} & = [& 0 & 0 & 0 & 0.3162 &]. \end{array}$$

Using equation (13) construct

$$\mathcal{N} = \begin{bmatrix} -0.3162 & 0 & 0 & 0 \\ -0.3162 & -0.3162 & 0.3162 & 0 \\ -0.3162 & -0.3162 & 0.3162 & 0.3162 \\ 0 & -0.3162 & 0.3162 & 0.3162 \\ 0 & 0 & 0 & 0.3162 \end{bmatrix}$$

and one can readily see that

$$\mathcal{N}[h_1, h_2]^{\mathrm{T}} = \mathbf{0}.$$

The matrix $\mathcal{N}$ contains the correct blurs in its null space. In real cases, when noise is present, we consider the l_2 norm as specified in equation (9).

In the course of $\mathcal{N}$'s derivation, we have to construct $\mathcal{G}$,which is huge even for images of moderate size, and then estimate its null space. However, efficient computation exists. The N smallest eigenvectors of $\mathcal{G}\mathcal{G}^{\mathrm{T}}$ give the null space matrix $\mathbf{N}$. The product $\mathcal{G}\mathcal{G}^{\mathrm{T}}$ is a square matrix of size proportional to E and can be calculated directly without first constructing $\mathcal{G}$; see e.g. [2] for details. E is the size of filters η and it is calculated from condition (11). It increases with the increasing SR factor ε and blur size H, but it decreases with the increasing number of LR images K. In general cases, the values of E are smaller or close to H. Therefore, the product $\mathcal{G}\mathcal{G}^{\mathrm{T}}$ is relatively small and the computation of $\mathcal{N}$ is fast.

3.3. Extension to color

There are three possible extensions of the acquisition model (1) to color images: assuming same blurs in color channels assuming different blurs in color channels and additionally assuming also intrachannel blurs between color channels ('crosstalks'). For the first two extensions, the PSF regularization term (9) can be used without any modifications. The third extension brings extra burden of crosstalks that prevents us from using the proposed PSF regularization and therefore we did not consider it here. Color channels are strongly correlated and it is highly desirable to introduce some coupling in the image regularization term (8). One can find a very good overview of different regularizations of color images in [28]. Here, we use the vector version of the variational approach, which is given by

$$Q(f) = \int \phi(\sqrt{\|\nabla f_r\|^2 + \|\nabla f_g\|^2 + \|\nabla f_b\|^2})dx\,dy,$$

where $f_{\mathrm{r}}, f_{\mathrm{g}}, f_{\mathrm{b}}$ are red, greed, blue channels, respectively. Correlation of colors is appropriately addressed by this term and we can use the same numerical computation as in the case of gray-scale images (see Section 3.1).

4. ALTERNATING MINIMIZATION

The complete energy function reads

$$E(\mathbf{f}, \mathbf{h}) = \sum_{k=1}^{K} \|\mathbf{D}_k\mathbf{H}_k\mathbf{f} - \mathbf{g}_k\|^2 + \alpha\mathbf{f}^{\mathrm{T}}\mathbf{L}\mathbf{f} + \mathbf{h}^{\mathrm{T}}(\beta\mathbf{L} + \gamma\mathcal{N}^{\mathrm{T}}\mathcal{N})\mathbf{h}. \quad (15)$$

To find a minimizer, we perform AMs of E over $\mathbf{f}$ and $\mathbf{h}$. The advantage of this scheme lies in its simplicity. Each term of equation (15) is quadratic and therefore convex (but not

necessarily strictly convex) and the derivatives w.r.t. $\mathbf{f}$ and $\mathbf{h}$ are easy to calculate. This AM approach is a variation on the steepest-descent algorithm. The search space is a concatenation of the blur subspace and the image subspace. The algorithm first descends in the image subspace and after reaching the minimum, i.e. $\nabla_{\mathbf{f}} E = 0$, it advances in the blur subspace in the direction $\nabla_{\mathbf{h}}$E orthogonal to the previous one, and this scheme repeats. In conclusion, starting with some initial $\mathbf{h}^0$ the two iterative steps are:

Step 1.

$$\begin{aligned} \mathbf{f}^m &= \arg\min_{\mathbf{f}} E(\mathbf{f}, \mathbf{h}^m) \\ &\Leftrightarrow \text{solve for } \mathbf{f} \\ &\left(\sum_{k=1}^{K} \mathbf{H}_k^{\mathrm{T}} \mathbf{D}_k^{\mathrm{T}} \mathbf{D}_k \mathbf{H}_k + \alpha \mathbf{L}\right) \mathbf{f} = \sum_{k=1}^{K} \mathbf{H}_k^{\mathrm{T}} \mathbf{D}_k^{\mathrm{T}} \mathbf{g}_k \,. \end{aligned} \tag{16}$$

Step 2.

$$\begin{aligned} \mathbf{h}^{m+1} &= \arg\min_{\mathbf{h}} E(\mathbf{f}^m, \mathbf{h}) \\ &\Leftrightarrow \text{solve for } \mathbf{h} \\ &([\mathbf{I}_K \otimes \mathbf{F}^{\mathrm{T}} \mathbf{D}_k^{\mathrm{T}} \mathbf{D}_k \mathbf{F}] + \gamma \mathcal{N}^{\mathrm{T}} \mathcal{N} + \beta \mathbf{L}) \mathbf{h} \\ &= [\mathbf{I}_K \otimes \mathbf{F}^{\mathrm{T}} \mathbf{D}_k^{\mathrm{T}}] \mathbf{g}, \end{aligned} \tag{17}$$

where $\mathbf{F} := \mathbf{C}_H^v\{f\}$, $\mathbf{g} := [\mathbf{g}_1^{\mathrm{T}}, \ldots, \mathbf{g}_K^{T}]^{\mathrm{T}}$ and m is the iteration step. Note that both steps consist of simple linear equations.

Energy E as a function of both variables $\mathbf{f}$ and $\mathbf{h}$ is not convex due to coupling of variables via convolution in the first term of equation (15). Therefore, it is not guaranteed that the BSR algorithm reaches the global minimum, instead, one may get trapped in local minima. In our experience, convergence properties improve significantly if we add feasible regions for the HR image and PSFs specified as lower and upper bounds constraints. To solve Step 1, we use the method of conjugate gradients (function *cgs* in Matlab) and then adjust the solution $\mathbf{f}^m$ to contain values in the admissible range, typically, the range of values of $\mathbf{g}$. It is common to assume that PSF is positive ($h_k \geq 0$) and that it preserves image brightness. We can therefore write the lower and upper bounds constraints for PSFs as $\mathbf{h}_k \in \langle 0,1 \rangle^{H^2}$. In order to enforce the bounds in Step 2, we solve equation (17) as a constrained minimization problem (function *fmincon* in Matlab) rather than using the projection as in Step 1. Constrained minimization problems are more computationally demanding but we can afford it in this case since the size of $\mathbf{h}$ is much smaller than the size of $\mathbf{f}$.

Parameters α, β and γ depend on the level of noise. If noise increases, α and β should increase, and γ should decrease. One can prove that α and β are proportional to σ_n^2, which is the noise variance. Estimation techniques, such as cross-validation [19] or expectation maximization [33], can be used to determine the correct weights. However, we did not want to increase the complexity of the problem any further and thus we set the values in experiments manually according to our visual assessment. If the iterative algorithm begins to amplify noise, we have underestimated the noise level. On contrary, if the algorithm begins to segment the image, we have overestimated the noise level.

5. EXPERIMENTS

The following experiments with the proposed BSR method aim to first compare performance with other techniques and second demonstrate its applicability to real scenarios with misregistered input images and non-integer SR factors.

5.1. PSNR performance

We evaluated noise robustness of the proposed BSR and compared it with other two methods: interpolation technique and state-of-the-art SR method. The former technique consists of the MBD method proposed in [7] followed by the standard bilinear interpolation resampling. The MBD method first removes volatile blurs and then the interpolation of the deconvolved image achieves the desired spatial resolution. The latter method, which we will call herein a 'standard SR method', is a MAP formulation of the SR problem proposed, in [12, 13]. This method uses a MAP framework for the joint estimation of image registration parameters (in our case only translation) and the HR image, assuming only the sensor blur ($\mathbf{U}$) and no volatile blurs. For an image prior, we used edge preserving

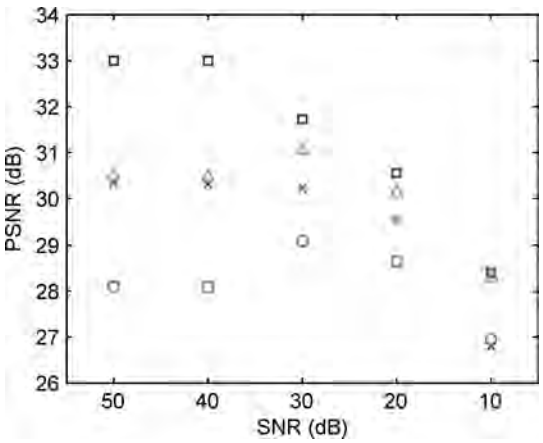

FIGURE 2. Performance of the BSR algorithm and the other two methods under different levels of noise: squares proposed BSR with $\beta = 0$; triangles proposed BSR with $\gamma = 0$; cross symbols represent MBD with bilinear interpolation; the circles represent the standard SR method. Note that the proposed BSR outperforms any other method but as the noise level increases its supremacy becomes less evident.

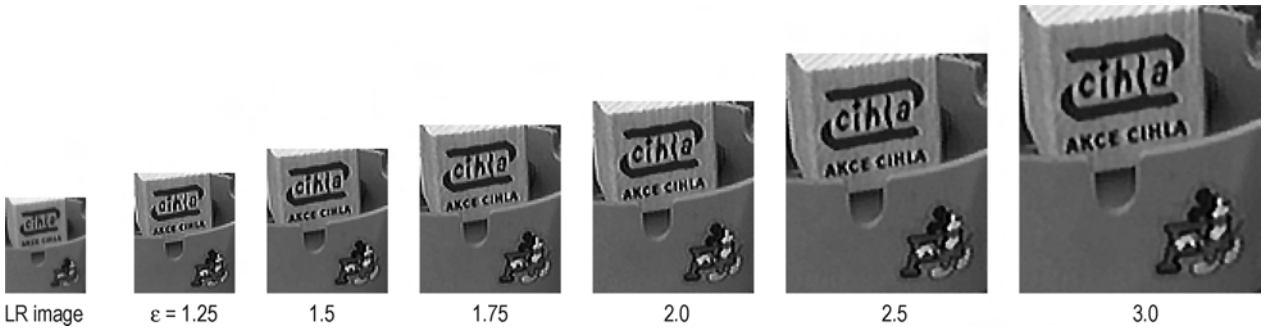

FIGURE 3. SR with non-integer factors of short-exposure images. The first left image is one of 10 LR frames acquired by a webcamera (exposure time 1/60 s) that were used to estimate HR images. The proposed BSR method was initialized with different SR factors from 1.25 to 3. The estimated HR images appear in their original size. An example of estimated PSFs for factor 2 is in Fig. 4.

Huber Markov random fields [34]. In order to evaluate the effect of the PSF regularization term (9), we ran the BSR method in two different modes. In the first mode, $\beta = 0$ and so the $\mathcal{N}$ term was considered. In the second mode, $\gamma = 0$ and so the standard smoothing term was considered.

The experimental setup was the following. First we generated six random motion blurs of size 4×4. Then we generated six LR images from the original 'Lena' image using the blurs and the downsampling factor of 2, and added white Gaussian noise with different signal-to-noise ratio (SNR) from 50 to 10 dB. SNR $= 10 \log(\sigma_f^2/\sigma_n^2)$, where σ_f and σ_n are the image and noise standard deviations, respectively. We repeated the whole procedure 10 times for different realizations of noise. For each set of six LR images, the three methods were applied one by one. Parameters of each method were chosen to minimize the mean square error of the HR estimate. Figure 2 summarizes the obtained results in terms of peak SNR defined as $\mathrm{PSNR}(\hat{\mathbf{f}}) = 10 \log\left(\frac{\mathrm{span(f)}^2}{\|\hat{\mathbf{f}} - \mathbf{f}\|^2/F^2}\right)$, where $\hat{\mathbf{f}}$ is the estimate of the original HR image $\mathbf{f}$, and span($\mathbf{f}$) denotes the span of gray-level values in the original image, typically 255.

The standard SR method gives the poorest performance, since it lacks any apparatus for removing volatile blurs. MBD with interpolation removes blurs in the LR domain, which accounts for better performance. However, the best performance is apparent for the proposed BSR method with $\mathcal{N}$ in the PSF regularization term. For low SNR, all the tested methods tend to give similar results in the PSNR perspective and advantages of the proposed BSR method are less evident. Thus, for very noisy images ($<$20 dB), it is sufficient to perform MBD with simple interpolation than to apply advance SR methods, since MBD is definitely faster and the results look similar due to noise.

5.2. Real data

We worked with a standard webcamera to record short video sequences of still scenes, extracted several consecutive frames and used the frames as input LR images. The input parameters of the BSR method were selected manually to give the best possible results. Common to all the experiments was the choice of the sensor blur, which was determined experimentally and was set to the Gaussian function of standard deviation $\sigma = 0.34$ (relative to the scale of LR images). One should underline that the proposed method is fairly robust to the underestimated size of the sensor blur, since it can compensate for insufficient variance by automatically including the missing factor of Gaussian functions in the volatile blurs. The quality of reconstructed HR images is not evaluated by any quantitative measure. Instead, we advocate the use of reader's subjective assessment.

The first experiment summarized in Figs. 3 and 4 compares results for different SR factors from 1.25 up to 3. In this case, the hand-held webcamera operated in good light conditions with the exposure time of 1/60 s and therefore no volatile blur was visible. Ten frames (see one such frame in the left side Fig. 3) extracted from the video served as input LR images for the BSR method with parameters $\alpha = 2 \times 10^{-3}$, $\gamma = 10$, $\beta = 0$, blur size 8×8 and six different SR factors $\varepsilon = 1.25,\ 1.5,\ 1.75,\ 2.0,\ 2.5,\ 3.0$. The HR images show improvement as the SR factor increases; however, the refinement becomes less visible after 2.0. The difference between 2.5 and 3.0 seems to be primarily only in size as no more details appear. In all the cases, estimated PSFs were more or less the same and an example for SR factor 2 is in Fig. 4. The PSFs are very localized and

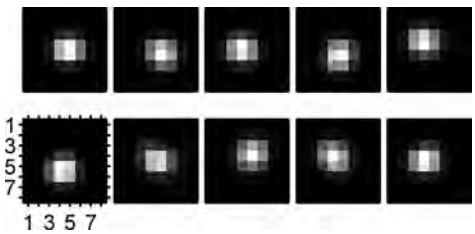

FIGURE 4. SR of short-exposure images. PSFs of LR images in Fig. 3 estimated by the proposed BSR method.

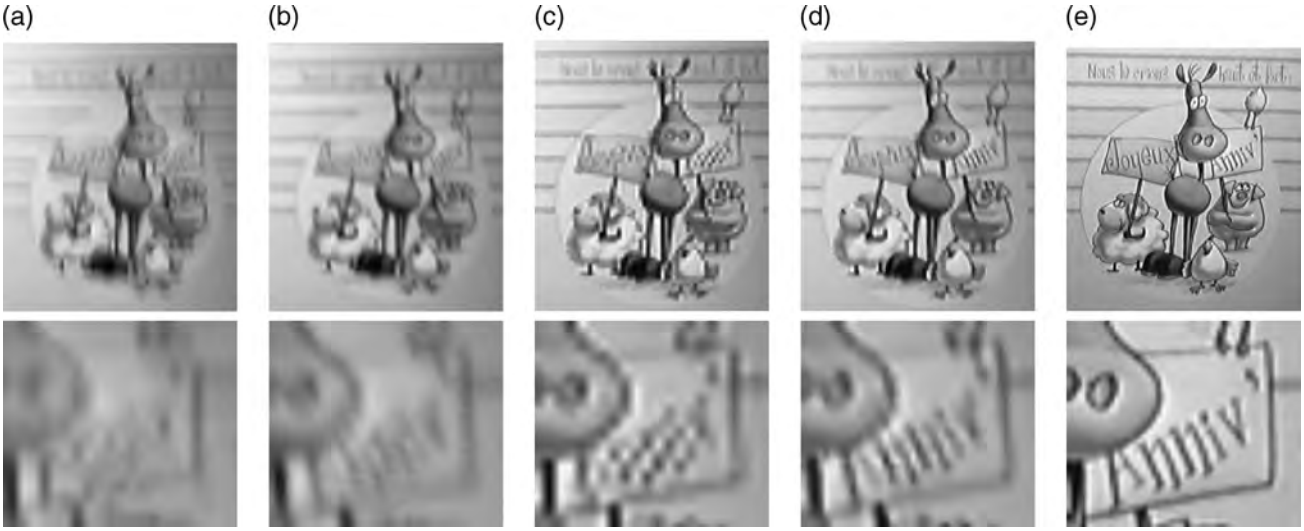

FIGURE 5. SR of long-exposure images. Five LR frames were extracted from a short video sequence captured by a webcamera (exposure time 1/10 s). An example of one frame and its close-up is in (a) top and bottom, respectively. The image is printed in the size of the output HR image for comparison reasons. Notice severe motion blur due to the long exposure time and motion of the hand-held camera. Estimated HR images for factor 5/3 were calculated by three different methods: standard SR in (b), MBD followed by bilinear interpolation in (c), and proposed BSR method in (d) (see PSFs estimated by BSR in Fig. 6). Compare obtained results with the image (e) acquired with the same webcamera but installed closer to the object.

they resemble delta functions (note that the displayed PSFs include the sensor blur), which was expected since the input images did not exhibit any volatile blur. Notice that the PSFs are shifted to compensate for subtle misalignments, which seamlessly performs subpixel registration and thus accurate SR.

In the second experiment, we recorded a greeting card with the hand-held webcamera in poor light conditions. The exposure time of the camera was 1/10 s and severe motion blur coming from the hand vibration is visible in images; see Fig. 5a. Then we move the camera toward the object, stabilize it, and grabbed one frame (Fig. 5e) to have an 'ideal' representation, which we show here only for evaluation reasons. Using five consecutive frames from the video, the HR image (SRF = 5/3) was estimated with three methods. The first result in Fig. 5b) was achieved by the standard SR method [13]. The result is poor as the method does not have means of removing blur. The second result in Fig. 5c shows MBD [7] with interpolation. The reconstructed image is sharper but many details are still missing, e.g. note the erroneous reconstruction of 'Anniv' on the flag held by the 'pig' right to the 'horse'. The third result is of the proposed BSR (Fig. 5d) run with parameters $\alpha = 2 \times 10^{-3}$ $\beta = 1$, $\gamma = 10$ and blur size 12×12. The obtained result after only three iterations of the AM algorithm is the sharpest with many details properly reconstructed. The key to successful reconstruction lies in the accurate estimation of PSFs within the iterative algorithm. As one could see in Fig. 6, the estimated PSFs model camera shake and since the whole procedure runs in the HR scale, the proposed method outperforms the former ones.

The third experiment demonstrates the advantage of using the decimation operators $\mathbf{D}_k$'s with registration instead of running BSR on registered LR images. A similar video sequence was recorded as in the previous case but this time we also rotated the camera during shooting to introduce geometric distortions that must be first eliminated by registration. An example of two such frames out of 10 is in Fig. 7a. Rotation is clearly visible and BSR cannot be applied without first registering the images. We estimated registration parameters and compared two approaches. First, we applied BSR on registered images; see the result in Fig. 7b. Second, we used the registration parameters to construct $\mathbf{D}_k$'s and applied BSR on the original unregistered images; see the result in Fig. 7c. In both cases, the parameters were set as in the previous experiment. Some small details are better reconstructed in the second approach, which indicates that using the registration parameters directly in BSR is preferable.

FIGURE 6. SR of long-exposure images. PSFs of images in Fig. 5(a) estimated by the proposed BSR method.

FIGURE 7. SR with registration. Ten frames were extracted from a video sequence recorded by a webcamera (exposure time 1/10 s). Two such frames are in (a) printed in the size of output HR images for comparison reasons. Due to slight rotation of the webcamera during shooting, registration parameters were first estimated by a registration method. Two approaches were compared: (b) Input frames were registered according to the parameters and BSR was applied on the registered images. (c) The registration parameters were used to modify decimation operators and BSR was applied to the original unregistered images. Better performance of the second approach is apparent from close-ups in the top row.

6. CONCLUSION

This paper presented an SR method for both integer and non-integer (rational) factors, which proved to be meaningful for cases when insufficient number of input LR images is available to perform SR with only integer factors, such as 2 or 3. To achieve truly robust methodology applicable in real situations, we adopted the regularized energy minimization approach, which we solve by alternating-minimization scheme. The fundamental improvement on previously proposed SR methods is the notion of estimating PSFs in the HR scale, which indirectly aligns LR images with subpixel accuracy. Using registration parameters inside, the algorithm instead of registering input images gives better results and paves the way for including methods of making registration parameters more accurate during reconstruction of the HR image [35].

FUNDING

Financial support of this research was provided by Czech Ministry of Education under the project 1M0572 (Research Center DAR), the Grant Agency of the Czech Republic under the project 202/05/0242, by the bilateral project 2004CZ0009 and by the projects TEC2004-00834, TEC2005-24739-E and PI040765.

REFERENCES

[1] Zitová, B. and Flusser, J. (2003) Image registration methods: a survey. *Image Vis. Comput.*, **21**, 977–1000.

[2] Harikumar, G. and Bresler, Y. (1999) Perfect blind restoration of images blurred by multiple filters: theory and efficient algorithms. *IEEE Trans. Image Process.*, **8**, 202–219.

[3] Giannakis, G. and Heath, R. (2000) Blind identification of multichannel FIR blurs and perfect image restoration. *IEEE Trans. Image Process.*, **9**, 1877–1896.

[4] Pai, H.-T. and Bovik, A. (2001) On eigenstructurebased direct multichannel blind image restoration. *IEEE Trans. Image Process.*, **10**, 1434–1446.

[5] Panci, G., Campisi, P., Colonnese, S. and Scarano, G. (2003) Multichannel blind image deconvolution using the bussgang algorithm: spatial and multiresolution approaches. *IEEE Trans. Image Process.*, **12**, 1324–1337.

[6] Šroubek, F. and Flusser, J. (2003) Multichannel blind iterative image restoration. *IEEE Trans. Image Process.*, **12**, 1094–1106.

[7] Šroubek, F. and Flusser, J. (2005) Multichannel blind deconvolution of spatially misaligned images. *IEEE Trans. Image Process.*, **14**, 874–883.

[8] You, Y.-L. and Kaveh, M. (1999) Blind image restoration by anisotropic regularization. *IEEE Trans. Image Process.*, **8**, 396–407.

[9] Rajagopalan, A. and Chaudhuri, S. (1999) An MRF model-based approach to simultaneous recovery of depth and restoration from defocused images. *IEEE Trans. Pattern Anal. Mach. Intell.*, **21**, 577–589.

[10] Park, S., Park, M. and Kang, M. (2003) Super-resolution image reconstruction: a technical overview. *IEEE Signal Process. Mag.*, **20**, 21–36.

[11] Farsui, S., Robinson, D., Elad, M. and Milanfar, P. (2004) Advances and challenges in super-resolution. *Int. J. Imag. Syst. Technol.*, **14**, 47–57.

[12] Hardie, R., Barnard, K. and Armstrong, E. (1997) Joint map registration and high-resolution image estimation using a sequence of undersampled images. *IEEE Trans. Image Process.*, **6**, 1621–1633.

[13] Segall, C., Katsaggelos, A., Molina, R. and Mateos, J. (2004) Bayesian resolution enhancement of compressed video. *IEEE Trans. Image Process.*, **13**, 898–911.

[14] Woods, N., Galatsanos, N. and Katsaggelos, A. (2006) Stochastic methods for joint registration, restoration, and interpolation of multiple undersampled images. *IEEE Trans. Image Process.*, **15**, 201–213.

[15] Farsiu, S., Robinson, M., Elad, M. and Milanfar, P. (2004) Fast and robust multiframe super resolution. *IEEE Trans. Image Process.*, **13**, 1327–1344.

[16] Shechtman, E., Caspi, Y. and Irani, M. (2005) Space–time super-resolution. *IEEE Trans. Pattern Anal. Mach. Intell.*, **27**, 531–545.

[17] Humblot, F. and Muhammad-Djafari, A. (2006) Super-resolution using hidden markov model and bayesian detection estimation framework. *EURASIP J. Appl. Signal Process.*, **2006**, 36971.

[18] Ben-Ezra, M. and Nayer, S. (2004) Notion-based motion deblurring. *IEEE Trans. Pattern Anal. Mach. Intell.*, **26**, 689–698.

[19] Nguyen, N., Milanfar, P. and Golub, G. (2001) Efficient generalized cross-validation with applications to parametric image restoration and resolution enhancement. *IEEE Trans. Image Process.*, **10**, 1299–1308.

[20] Woods, N., Galatsanos, N. and Katsaggelos, A. (2003) EM-based simultaneous registration, restoration, and interpolation of super-resolved images. *Proc. ICIP*, Barcelona, September, pp. 303–306. IEEE Computer Society.

[21] Rajan, D. and Chaudhuri, S. (2003) Simultaneous estimation of super-resolved scene and depth map from low resolution defocused observations. *IEEE Trans. Pattern Anal. Mach. Intell.*, **25**, 1102–1117.

[22] Šroubek, F. and Flusser, J. (2006) Resolution enhancement via probabilistic deconvolution of multiple degraded images. *Pattern Recognit. Lett.*, **27**, 287–293.

[23] Chen, Y., Luo, Y. and Hu, D. (2005) A general approach to blind image super-resolution using a PDE framework. *Proc. SPIE*, Beijing, July, pp. 1819–1830. SPIE.

[24] Wirawan, D.P. and Maitre, H. (1999) Multi-channel high resolution blind image restoration. *Proc. ICASSP*, Phoenix, AR, March, pp. 3229–3232. IEEE Computer Society.

[25] Yagle, A. (2003) Blind superresolution from under-sampled blurred measurements. *Proc. SPIE*, Bellingham, December, pp. 299–309. SPIE.

[26] Biggs, D., Wang, C.L., Holmes, T. and Khodjakov, A. (2004) Subpixel deconvolution of 3D optical microscope imagery. *Proc. SPIE*, Denver, CO, October, pp. 369–380. SPIE.

[27] Šroubek, F., Cristóbal, G. and Flusser, J. (2007) A unified approach to superresolution and multichannel blind deconvolution. *IEEE Trans. Image Process.*, **16**, 2322–2332.

[28] Tschumperlé, D. (2002) PDE's-based regularization of multivalued images and applications. PhD Thesis, University of Nice-Sophia Antipolis.

[29] Lin, Z. and Shum, H.-Y. (2004) Fundamental limits of reconstruction-based superresolution algorithms under local translation. *IEEE Trans. Pattern Anal. Mach. Intell.*, **26**, 83–97.

[30] Pelletier, S. and Cooperstock, J. (2007) Fast super-resolution for rational magnification factors. *Proc. ICIP*, San Antonio, TX, September, pp. 65–68. IEEE Computer Society.

[31] Šroubek, F., Flusser, J. and Cristóbal, G. (2007) Multiframe Blind Deconvolution Coupled with Frame Registration and Resolution Enhancement. In Campisi, P. and Egiazarian, K. (eds.), *Blind Image Deconvolution: Theory and Applications*. CRC Press, FL.

[32] Aubert, G. and Kornprobst, P. (2002) *Mathematical Problems in Image Processing*. Springer, New York.

[33] Molina, R., Vega, M., Abad, J. and Katsaggelos, A. (2003) Parameter estimation in Bayesian highresolution image reconstruction with multisensors. *IEEE Trans. Image Process.*, **12**, 1655–1667.

[34] Capel, D. (2004) *Image Mosaicing and Super-Resolution*. Springer, New York.

[35] Chung, J., Haber, E. and Nagy, J. (2006) Numerical methods for coupled super-resolution. *Inverse Probl.*, **22**, 1261–1272.